Biointerface Research in Applied Chemistry
Open-Access Journal (ISSN: 2069-5837)

*Article*
**Volume 13, Issue 2, 2023, 165**
https://doi.org/10.33263/BRIAC132.165

# Effect of Low-Doping Concentration on Silver-Doped $SnO_2$ and its Photocatalytic Applications

**Hassan Adebayo Shittu** [1], **Oluwaseun Adedokun** [1,2,*], **Maroof Alade Kareem** [1], **Paramasivam Sivaprakash** [4], **Ismaila Taiwo Bello** [1,3,*], **Sonachalam Arumugam** [4]

[1] Department of Pure and Applied Physics, Ladoke Akintola University of Technology, Ogbomoso, Nigeria; kareemmaroof@gmail.com (M.A.K.); harzanshi2@gmail.com (H.A.S.); oadedokun@lautech.edu.ng (O.A.);
[2] Nanotechnology Research Group (NANO$^+$), Ladoke Akintola University of Technology, Ogbomoso, Nigeria; oadedokun@lautech.edu.ng (O.A.);
[3] Department of Physics, College of Science, Engineering and Technology, University of South Africa, Johannesburg 1710, South Africa; ismailbello26@gmail.com (I.T.B.);
[4] Centre for High Pressure Research, School of Physics, Bharathidasan University, Tiruchirappalli 620 024, Tamil Nadu, India, shiva.kutty820@gmail.com (P.S.); sarumugam1963@bdu.ac.in (S. A.);
* Correspondence: oadedokun@lautech.edu.ng (O.A.); ismailbello26@gmail.com (I.T.B.)

Scopus Authors ID 57190128209 (O.A.); 57202357845 (I.T.B)

**Received: 31.01.2022; Accepted: 4.03.2022; Published: 29.03.2022**

**Abstract:** Stannic Oxide ($SnO_2$) is in the class of metal oxide semiconductors, which is widely employed in a series of applications because of its excellent electrical and optical properties. In this study, we reported the synthesis of undoped and silver (Ag) doped $SnO_2$ via a simple coprecipitation technique to study the photocatalytic activities of Ag/$SnO_2$. Different characterization techniques, such as XRD, SEM, EDX, FTIR, RAMAN, and DRS were used to study the effect of the doping concentration of Ag on the structural, morphological, compositional, and optical properties of $SnO_2$. The XRD spectrum showed the tetragonal structure of $SnO_2$ and Ag/$SnO_2$. The SEM micrographs show the irregular distribution of particles with different shapes and sizes. The EDX results show the incorporation of the Ag element into $SnO_2$. The optical property shows narrowed bandgap energy with Ag content. The photocatalytic activity of the samples was studied by the photocatalytic degradation of Methylene Blue (MB) dye. The photocatalytic activity results reveal that 1wt% of Ag/$SnO_2$ has a better photocatalytic performance of 97.63% when compared to undoped $SnO_2$.

**Keywords:** silver doping; metal oxide; stannic oxide; coprecipitation; photocatalyst; methylene blue die.



## 1. Introduction

The severity of the persistent increase of organic pollutants that emanates from households and industrial effluents poses a great threat to both aquatic and human life [1–3]. Methylene blue (MB) dye is majorly employed in different industrial applications with core applications in textile industries. MB is mostly used for coloring silk, wood, sticks, paper, and cotton [4]. It has also been used in coloring drugs and cosmetics in aqueous drug solutions. The discharge of these dyes causes effluents to water which is harmful to both domestic and aquatic life [5,6]. Over the last decades, different methods have been established and used to degrade such pollutants from different sources. Most methods employed to purify wastewater are flocculation, coagulation, precipitation,

adsorption, ion exchange, and membrane processing [7,8]. However, numerous progress has been recorded in this field. The majority of these approaches are usually impossible for large-scale applications. Most of these methods are costly and do not degrade the toxic materials completely, hence generating a lesser toxic product [9,10]. To remove organic contaminants from water, a photocatalytic Advanced Oxidation Process (AOP) is used to alleviate major environmental concerns [11,12]. The mechanism of this process is the generation of hydroxyl radicals (OH*) on the surface of the catalyst, which oxidatively degrades the pollutant existing in the sample. Metal oxides semiconductors, such as $SnO_2$, $TiO_2$, and ZnO, have been the promising choice of researchers for elementary research and practical applications due to their chemical inertness, high activity, non-toxicity, and low cost [13–19].

Among various metal-oxide-semiconductor that have been employed as a photocatalyst, stannic oxide ($SnO_2$) nanoparticle, a natural n-type semiconductor with a bandgap of 3.6eV, have been projected to be a strong photocatalyst for the degradation of organic pollutants owing to its unique properties, for instance, high transparency, cost-effectiveness, high photosensitivity and environmental friendliness [20–23]. Compared with other metal oxide semiconductors, the photocatalytic efficiency of $SnO_2$ is low because of its wide bandgap, limiting its light absorption to irradiation wavelength to the ultraviolet (UV) region of the electromagnetic spectrum but not in the visible region. Consequently, the rapid recombination of generated electron/hole ($e^-/h^+$) pairs is another factor limiting these metal oxide semiconductors in photocatalysis [9,24]. Therefore, there has been much research interest in overcoming these challenges, thereby enhancing the photocatalytic activity of metal oxides. Researchers' efforts have been tailored to develop visible-light-assisted photocatalysts; such methods have been employed to modify $SnO_2$, such as doping with semiconductors, metal, non-metals, and noble metals. But doping $SnO_2$ with noble metals shown to be more promising, such as Cu, Au, Ag, etc. [13,25–29]. Doping $SnO_2$ with a silver (Ag) may hinder recombination of the electron/hole pair and also can be used to reduce the bandgap of undoped $SnO_2$ [30]. In addition, Ag is more desirable and attractive due to its non-toxicity, cost-effectiveness, and work function Ag aid the formation of a desirable band alignment. Ag-doped photocatalyst has a remarkable photocatalytic performance under solar irradiation, which might be due to the surface plasmon resonance of Ag under visible light irradiation [17,31–33].

Recently, Ag/$SnO_2$ has been successfully synthesized and employed as a photocatalyst in removing organic pollutants using different synthesis methods. However, most of the reported work centered on the higher doping concentration of Ag [7,11,13,15,22]. Hence it is essential to study the effect of the lower doping concentration of Ag on $SnO_2$ and its efficacy as a photocatalyst for the degradation of Methylene Blue (MB) dye. In addition, different methods have been adopted for the synthesis of Ag/ $SnO_2$, such as hydrothermal, solvothermal, sol-gel, coprecipitation, thermal evaporation methods, among others [17,31,34–37]. But coprecipitation is proven relatively simple and effective owing to its advantages of easy and rapid synthesis seamless control of particle size, composition, and morphology [38,39].

This study synthesized undoped and Ag-doped $SnO_2$ using the coprecipitation technique. The photocatalytic activities of the synthesized samples were investigated and compared. In addition, the effect of low concentration Ag doping on the photocatalyst was investigated.

## 2. Materials and Methods

Tin (II) chloride dehydrate ($SnCl_2.H_2O$), and silver nitrate ($AgNO_3$) procured from Sigma Aldrich and Merck Chemicals, India, were used as sources of tin and silver, respectively. Distilled water was used as a solvent for synthesis. Ammonia was used as a precipitate agent to get the desired pH value. All the chemicals and solvents used are analytical grade.

### *2.1. Preparation of $SnO_2$ and Ag-doped $SnO_2$.*

Ag/$SnO_2$ was prepared by dissolving 5.21g (0.077M) of Tin (II) chloride dihydrate in 300ml of distilled water. The solution was stirred in a magnetic stirrer for 20 minutes to obtain a homogeneous solution. Concentration of $AgNO_3$ at different atomic ratio (0.25, 0.50, 0.75 and 1 %) were added to the solution. Consequently, aqueous ammonia as a precipitate agent dropped wisely added to the solution under vigorous stirring until a pH of 12 is attained. The precipitate formed was centrifuged for 10 minutes at 2000 rpm to completely remove organic materials ($Cl^-$ and $NO_3^-$) ions at the surface; the sediment was washed with distilled water and soaked in ethanol for 2 hours, and then centrifuged for 10minutes to remove the ethanol. The precipitate obtained was dried for 4 hours at a temperature of 80$^o$C, and after grinding, the powder was annealed for 2 hours at 500$^o$C; a yellowish-colored powder was obtained. The above procedure was repeated to prepare the pure $SnO_2$ without adding $AgNO_3$, which resulted in a white powdered $SnO_2$.

### *2.2. Characterization of the samples.*

The samples' grain size and crystallography were studied using a powdered X-ray technique by Rigaku X-ray diffractometer with monochromatic Cu Kβ with wavelength (λ= 1.5406Å) at 40kV and 30mA. The scanning speed of all samples was 2.0156° at the scanning range of 10° - 80°. The morphological and elemental composition analysis was obtained in (FESEM) model 6340F (JEOL Japan) coupled with (EDX Model INCA 200 (UK)) at 20 keV. The organic, inorganic, and polymeric nature of the samples were studied using a PerkinElmer FTIR spectrometer. The Raman spectra were recorded using an (STR 500 Cornes Technology) Raman spectroscopy machine (Japan) having 100x objective of the microscope at an excitation wavelength of 514.5 nm. Iron (Fe) green laser was used to excite the samples at approximately 50 mW. The Raman signal was collected in the spectral interval of 150 $cm^{-1}$ until 3500 $cm^{-1}$. The Raman shift and intensities of the scattered light were compared with reference data. The diffuse absorbance and reflectance spectra were obtained using Ocean Optics USB 4000 in the range of 200-900 nm. The DRS spectrum was used to calculate the energy bandgap using the Kubelka-Munk relation, as shown in equation 1.

$$F(R) = \frac{(1-R)^2}{2R} \qquad (1)$$

where R is the reflectance, F(R) is proportional to the extinction coefficient (α).

### *2.3. Photocatalytic activity.*

Photocatalytic activity of the synthesized nanoparticles was conducted to degrade a modeled methylene blue (MB) dye in the presence of sunlight. The solar spectrum measured on

an experimental day with a Lux meter was 90,000lux. At a neutral pH, 2.5mol/L of the dye solution was prepared in a volumetric flask. 25mL of the dye solution was measured in a 250mL flask. To every 25 mL of dye solution, 15 mg photocatalyst was added and stirred for 20 minutes to achieve the adsorption/desorption equilibrium and later exposed to solar irradiation for 120 mins. At specified time intervals (0 min, 15min, 30 min, 45 min, 60 min, 75min, 90 min, 105 min, and 120 min) 2 ml of the samples was extracted and centrifuged for 5 minutes to remove the photocatalyst. The supernatant was studied by a UV-visible spectrophotometer to monitor changes in the absorbance peaks for calculating the degradation percentages using Beer's Lambert equation as shown in equation 2.0.

$$\% \text{ Degradation} = \frac{Co - Ct}{Co} \times 100 \qquad (2)$$

where $C_o$ is the initial concentration of MB dye and $C_t$ is the concentration of dye solution after exposure time (t) to solar light.

## 3. Results and Discussions

### *3.1. X-ray diffraction analysis of $SnO_2$ and Ag/$SnO_2$.*

The crystal structure of the synthesized samples via coprecipitation techniques was analyzed by the XRD spectrum of $SnO_2$ and Ag/$SnO_2$. As shown in figure 1, the undoped $SnO_2$ exhibits a well-defined tetragonal structure at the diffraction peaks at 26.51°, 34.56°, 38.62°, 52.82°, 55.81°, 58.62°, 62.03°, 64.71°, 65.84°, 71.24°, 78.22° with diffraction plane (110), (101), (200), (211), (220), (002), (310), (112), (301), (202) and (321) matched with JCPDS card number (No: 41-1445). A notable peak of low intensity at 33.54° 2theta degree matched with JCPDS card number (No: 07-0483) was observed, which increases as the concentration of the dopant increases.

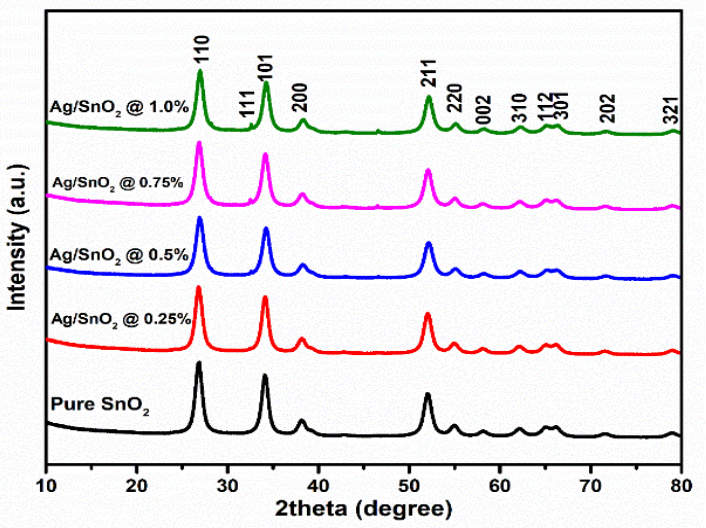


**Figure 1.** (**a**) XRD spectrum of pure $SnO_2$, 0.25, 0.5, 0.75 and 1.0 at% Ag/ $SnO_2$.

The incorporation of Ag nanoparticles gradually shifts the most intense peak (110) towards a higher 2theta degree. However, the shift is inconsistence, 0.25 and 0.5% Ag/$SnO_2$ nanoparticles shifted to a higher 2theta degree, but 0.75% Ag/ $SnO_2$ shifted back to a lower 2theta degree while 1% Ag/$SnO_2$ nanoparticles shifted to a higher 2theta degree as it was observed in the XRD pattern

revealed in Figure 2a. This confirms that Ag is successfully loaded into the $SnO_2$ lattice. The crystallite of the samples was calculated using Scherer's equation, as shown in equation 3. Where D is crystallite size, β is full width at half maxima (FWHM), θ is the glancing angle, and 0.98 is the shape factor.

$$D = \frac{0.98\lambda}{\beta Cos\theta} \qquad (3)$$

Figure 2b shows the mean crystalline size are in the range 9.08, 8.47, 9.57, 12.65, and 19.95 nm respectively for undoped $SnO_2$ and Ag/ $SnO_2$ concentration at 0.25, 0.5, 0.7%, and 1%. The increase in the crystallite sizes of 1% Ag doped $SnO_2$ might be a result of the segregation of Ag ions in the $SnO_2$ boundaries.

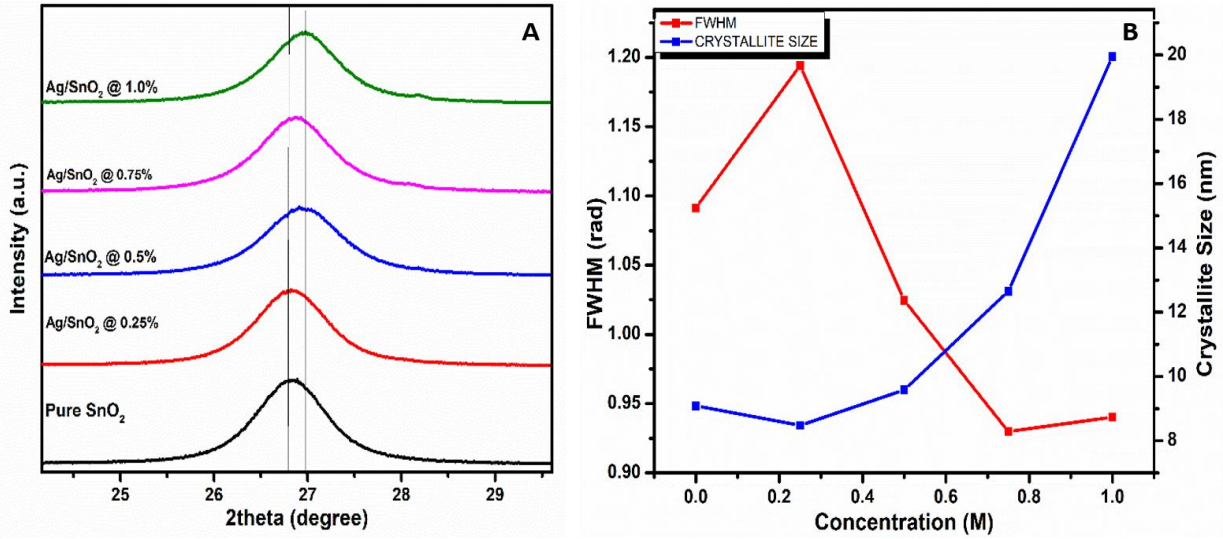


**Figure 2.** (**a**) Magnified XRD spectra of 110 peaks; (**b**) Change in Full-Width Half Maximum and Crystallite size of the synthesized samples

*3.2. Structural and morphological analysis of the samples.*

Field Emission Scanning Electron Microscope (FESEM) has been used to investigate the effect of Ag doping on $SnO_2$. Figure 3(a-c) below shows the morphological images of undoped $SnO_2$, 0.5 and 1.0 at% Ag/$SnO_2$ photocatalyst. The FESEM micrograph shows that the particles are irregularly distributed, and they vary in size and occur as the tetragonal structure of $SnO_2$ [40]. The tetragonal structure of the particle is in good agreement with the XRD result.

**Table 1.** Atomic and weight concentration (%) of the synthesized nanoparticles.

| Samples | Elements | Atomic % | Weight % | Kev |
|---|---|---|---|---|
| **$SnO_2$** | Sn | 78.97 | 66.39 | 3.6 |
| | O | 21.03 | 33.61 | 0.8 |
| **0.5% Ag/$SnO_2$** | Sn | 19.15 | 62.99 | 3.6 |
| | O | 80.39 | 35.65 | 0.6 |
| | Ag | 0.46 | 1.37 | 2.7 |
| **1% Ag/$SnO_2$** | Sn | 25.55 | 70.24 | 3.6 |
| | O | 73.43 | 27.21 | 0.6 |
| | Ag | 1.02 | 2.54 | 2.6 |

The micrograph distinctly specifies the occurrence of agglomeration and also affirms that the morphology of the undoped $SnO_2$ and Ag/$SnO_2$ are similar. The elemental composition of the

selected samples as shown by the EDX spectra in Figure 3(d-f), the pattern in Figure 3(d) reveal that the undoped $SnO_2$ sample consists of Sn and O atoms only, the absence of no other element revealed the purity of the synthesized sample.

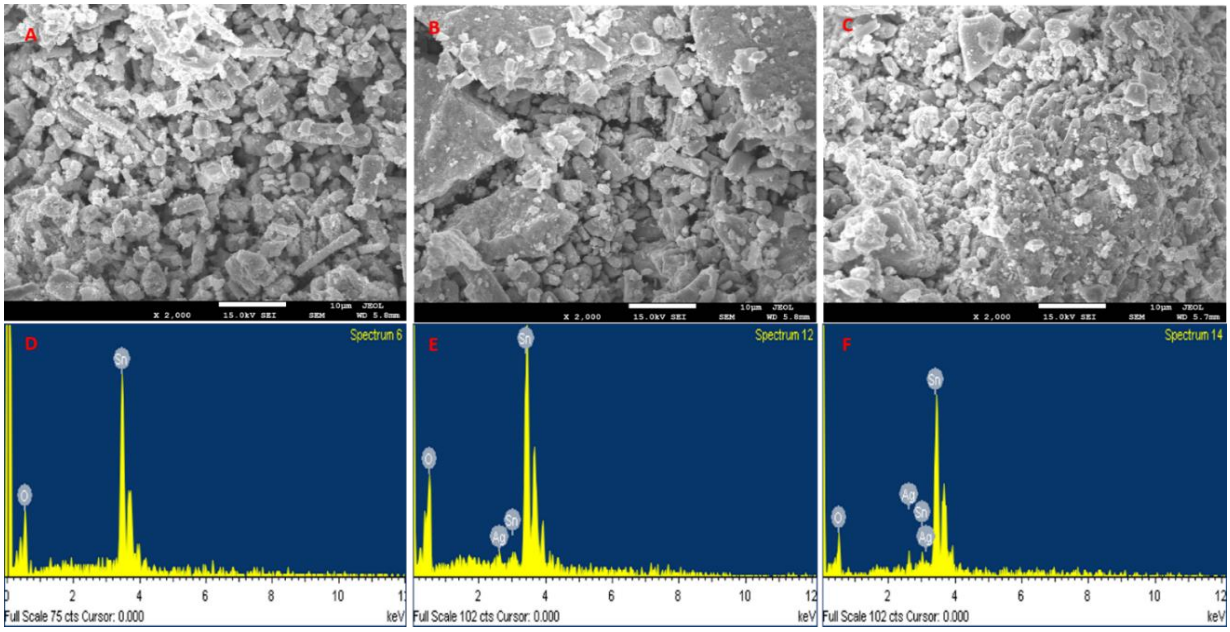


**Figure 3.** SEM and EDX spectrum of (**a & d**) Undoped $SnO_2$ (**b & e**) 0.5 Ag/ $SnO_2$ (**c & f**) 1.0 Ag/ $SnO_2$.

Figure 3(e and f) are the EDX spectra of 0.5 and 1 % of Ag/$SnO_2$, and they contain Sn, O, and Ag, respectively, which implies that Ag is successfully incorporated into $SnO_2$. The absence of any other element confirms the purity of the synthesized samples. The weight and atomic percentage of those samples, as revealed by the EDX analysis, are shown in Table 1.

*3.3. Optical characteristics of $SnO_2$ and Ag/ $SnO_2$.*

The optical characteristic of the undoped $SnO_2$ and Ag-doped $SnO_2$ as revealed by diffuse reflectance scattering (DRS) in the scanning range of 200-900nm is shown in Figure 4. In Figure 4a, the absorbances spectra for the undoped $SnO_2$ appeared at 302.3 nm.

**Table 2.** Absorption maxima, energy band gap and crystallite size of the undoped and Ag doped $SnO_2$ NPs.

| Name of Sample | Undoped $SnO_2$ | 0.25% Ag/$SnO_2$ | 0.5% Ag/$SnO_2$ | 0.75% Ag/$SnO_2$ | 1% Ag/$SnO_2$ |
|---|---|---|---|---|---|
| **Absorption maxima (nm)** | 302.3 | 299.2 | 301.0 | 301.8 | 292.8 |
| **Energy band gap $E_g$ (eV)** | 3.36 | 3.25 | 3.19 | 3.10 | 3.05 |
| **Crystallite Size (nm)** | 9.08 | 8.47 | 9.57 | 12.65 | 19.95 |

As the doping concentration increases (i.e. 0.25, 0.5, 0.75, and 1.0%) the absorption peaks also have a blue shift to 299.2, 301.0, 301.8 and 292.8nm respectively. The addition of Ag content could be responsible for the blue shift in the absorbance spectra, which correlates with the report of Yakout's works [41]. Figure 4b is the reflectance spectra of the synthesized samples; there is a redshift with the addition of a dopant. The optical band gap calculation was determined by the Kubelka-Munk relation. The graph of $(F(R)hv)^2$ was plotted against the photon energy, and the intercepts of the graph give the bandgap energy. The bandgap energy was found to be 3.36, 3.25,

3.18, 3.10, and 3.05 for the undoped and 0.25, 0.5, 0.75, and 1.0% Ag doped $SnO_2$, respectively, as shown in Table 2 and Figure 4.

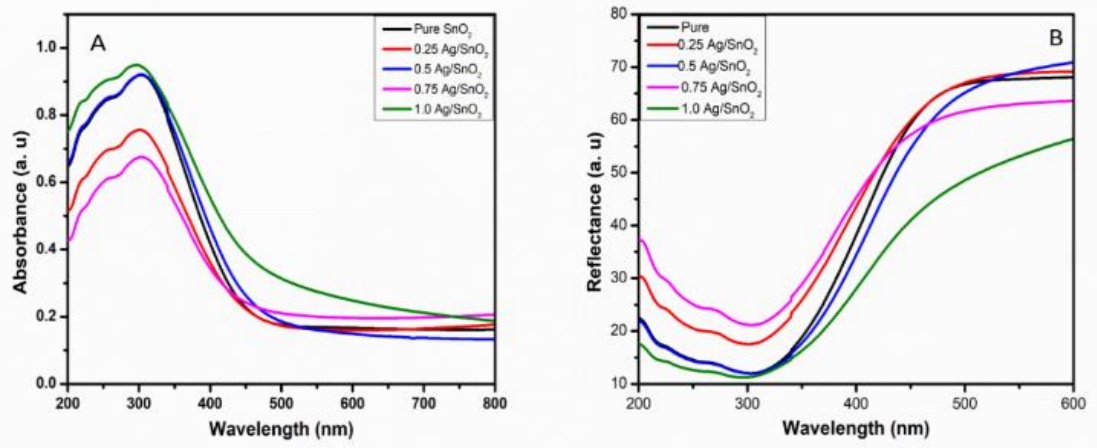


**Figure 4.** Absorbance and Reflectance spectra pure and Ag-doped $SnO_2$.

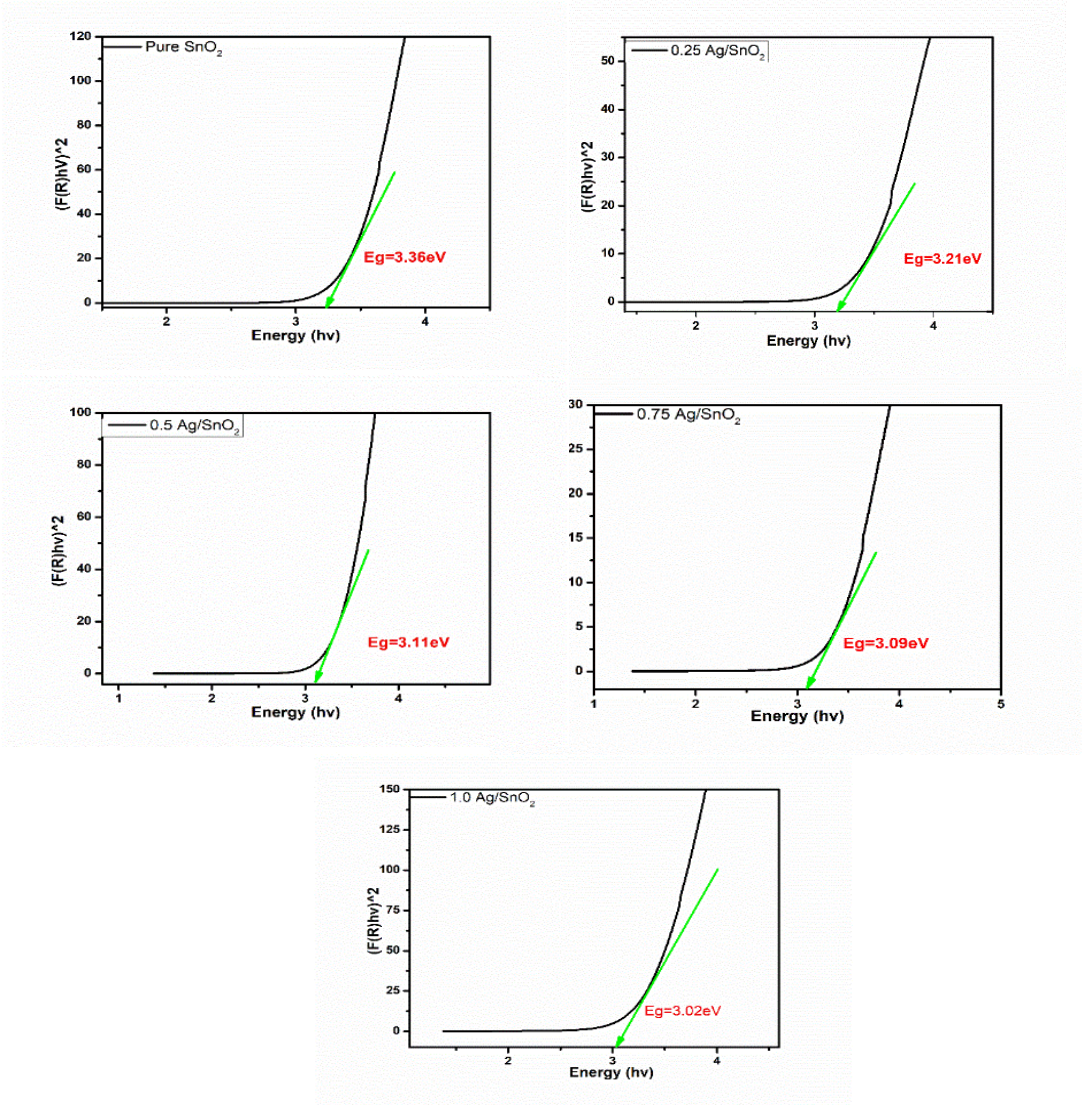


**Figure 5.** Estimated energy bandgap plot for undoped and Ag-doped $SnO_2$ NPs.

*3.4. FTIR analysis.*

The functional group of the synthesized samples was verified using FTIR analysis. The FTIR spectra obtained from the synthesized $SnO_2$ and $Ag/SnO_2$ were as shown in Figure 6. The IR spectrum of undoped $SnO_2$ nanoparticles is located at bands 3438, 1628, 973, and 642 $cm^{-1}$. The FTIR band at 3438 $cm^{-1}$ was ascribed to O–H stretching vibration, showing a hydroxyl group. The occurrence of a predominant peak at the 642 $cm^{-1}$ FTIR band was related to metal-oxygen (M-O) bonds which corroborate with the report of Kumar *et al.*, 2015 [42]. The band at 1623 $cm^{-1}$ can be associated with the stretching vibration of surface and interlayer hydroxyl groups (O-H bond) [43].

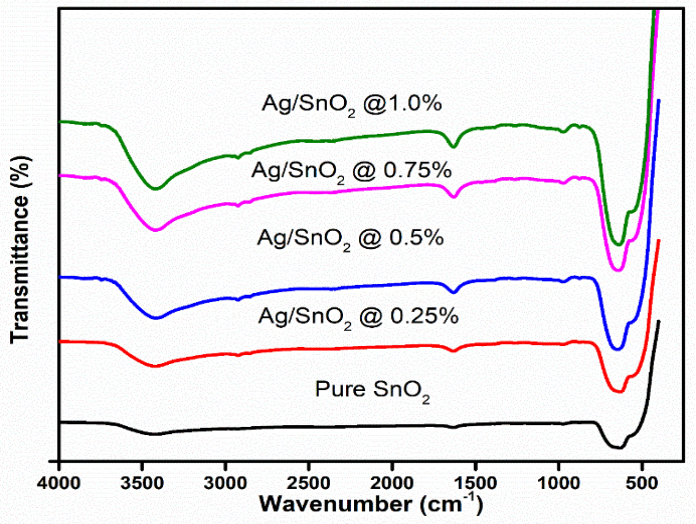


**Figure 6.** FTIR spectrum of $SnO_2$ and $Ag/SnO_2$ nanoparticles.

*3.5. Raman spectroscopy.*

The Raman analysis of the pure $SnO_2$ and $Ag/SnO_2$ nanoparticles was investigated using a Raman system to determine the variety of phonons and synthesized samples' crystallography. The data obtained were in the wavenumber range of 200 - 850 $cm^{-1}$, as shown in Figure 7. The Raman spectrum analysis reveals three peaks in-line with the report for $SnO_2$ crystals.

Peaks at around 633 ($cm^{-1}$) could be assigned to $A_{1g}$, which is symmetric Sn–O stretching, and peaks at around 775 ($cm^{-1}$) could be assigned to $B_{2g}$, which is asymmetric Sn–O stretching, respectively, which correspond to the tetragonal structure of $SnO_2$ [28]. It is clearly observed that Raman peaks increase as the doping concentration increase while peaks of 0.75% Ag/ $SnO_2$ decrease. Remarkably, the band at around 553 ($cm^{-1}$) may be attributed to the vibration mode associated with the vacant site and local order disorder. The addition of dopant introduced a peak around 234 ($cm^{-1}$), which increases as the doping concentration increases. Generally, peaks of $A_{1g}$ and $B_{2g}$ are virtual to the contraction and expansion vibrational modes of Sn-O bonds [28], and the existence of these Raman characteristics measures the tetragonal structure of SnO2. The change in the symmetric and asymmetric Sn-O stretching of the Ag-doped $SnO_2$ nanoparticle may enhance its photocatalytic performance.

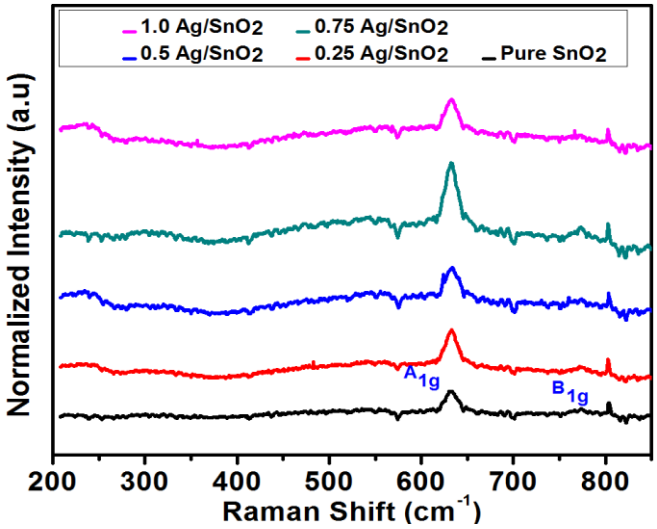


**Figure 7.** Raman spectrum of pure $SnO_2$ and $Ag/SnO_2$ nanoparticles.

*3.6. Photocatalytic activity.*

The photocatalytic activities of $SnO_2$ and $Ag/SnO_2$ were recorded by the degradation of MB dye under solar light irradiation. Figure 8 (a-e) shows the absorption spectra of an aqueous solution of 25ml MB with 15mg of the different photocatalysts under solar light irradiation for various time intervals. It can be observed that the absorption peaks decrease rapidly with an increase in the exposure time, indicating the degradation of MB. The UV-Vis absorbance spectrum was recorded in the range of 190 to 800 nm, and absorbance maxima were observed at 664 nm. The absorption of MB at 664 nm continuously decreases, and the peak is almost disappeared within 120 min.

It was observed in Figure 9 that the photodegradation efficiency of $SnO_2$ got enhanced with Ag doping; the 1% $Ag/SnO_2$ photocatalyst showed a maximum efficiency of 97.63% among the doped samples. The photocatalytic degradation efficiency of undoped and Ag-doped $SnO_2$ over MB are in the range of 86.89, 94.21, 96.68, 96.30 and 97.63% for undoped $SnO_2$, 0.25% $Ag/SnO_2$, 0.5% $Ag/SnO_2$, 0.75% $Ag/SnO_2$ and 1% $Ag/SnO_2$, respectively as calculated using Beer-Lambert equation. The amount of Ag-doped $SnO_2$ surface is an essential factor optimized to achieve enhanced photocatalytic performance. The effective charge transferability, visible light-harvesting ability, provision of catalytic sites for OH formation also injection of electrons into the $SnO_2$ surface by Ag ions could be accountable for the improved photocatalytic performance of the doped samples [44]. Moreover, the rate constant (k) was calculated by applying a first-order kinetic reaction. And figure 10 compares the photocatalyst's behavior under dark conditions and when it is exposed to visible light.

Also, Table 3 compares the existing literature with the present work, where it is noticed that this present study is very promising in the degradation of organic pollutants.

**Table 3.** Comparison of existing work with this present work on $Ag/SnO_2$ photocatalyst.

| Synthesis method | Photocatalyst (mol/wt%) | Dye | Degradation (%) | Time (min) | References |
|---|---|---|---|---|---|
| Hydrothermal | $Ag/SnO_2$-g-$C_3N_4$ | RhB | 94 | 240 | [45] |
| Hydrothermal | $Ag/SnO_2$ | Nitrogen Oxide | 70 | 30 | [34] |
| Soft Chemical route | $Ag/SnO_2$ (0, 5, 10, 15%) | MO | 93.44 | 180 | [46] |

| Synthesis method | Photocatalyst (mol/wt%) | Dye | Degradation (%) | Time (min) | References |
|---|---|---|---|---|---|
| Co-precipitation | Ag/$SnO_2$ | Rose bengal | 85.3 | 150 | [17] |
| Hydrothermal | Ag/$SnO_2$ (10%) | Rhodamine Blue (RhB) | 92 | 240 | [47] |
| Hydrothermal | Ag/$SnO_2$ nanowires | RhB | 93 | 35 | [48] |
| Microwave Irradiation | Ag/$SnO_2$ (5%) QDs | Methylene Blue | 97.5 | 120 | [31] |
| Coprecipitation | Ag/$SnO_2$ (0-1%) | 25ml/15mg, 2.5mol/L MB | 97.63 | 120 | Present work |

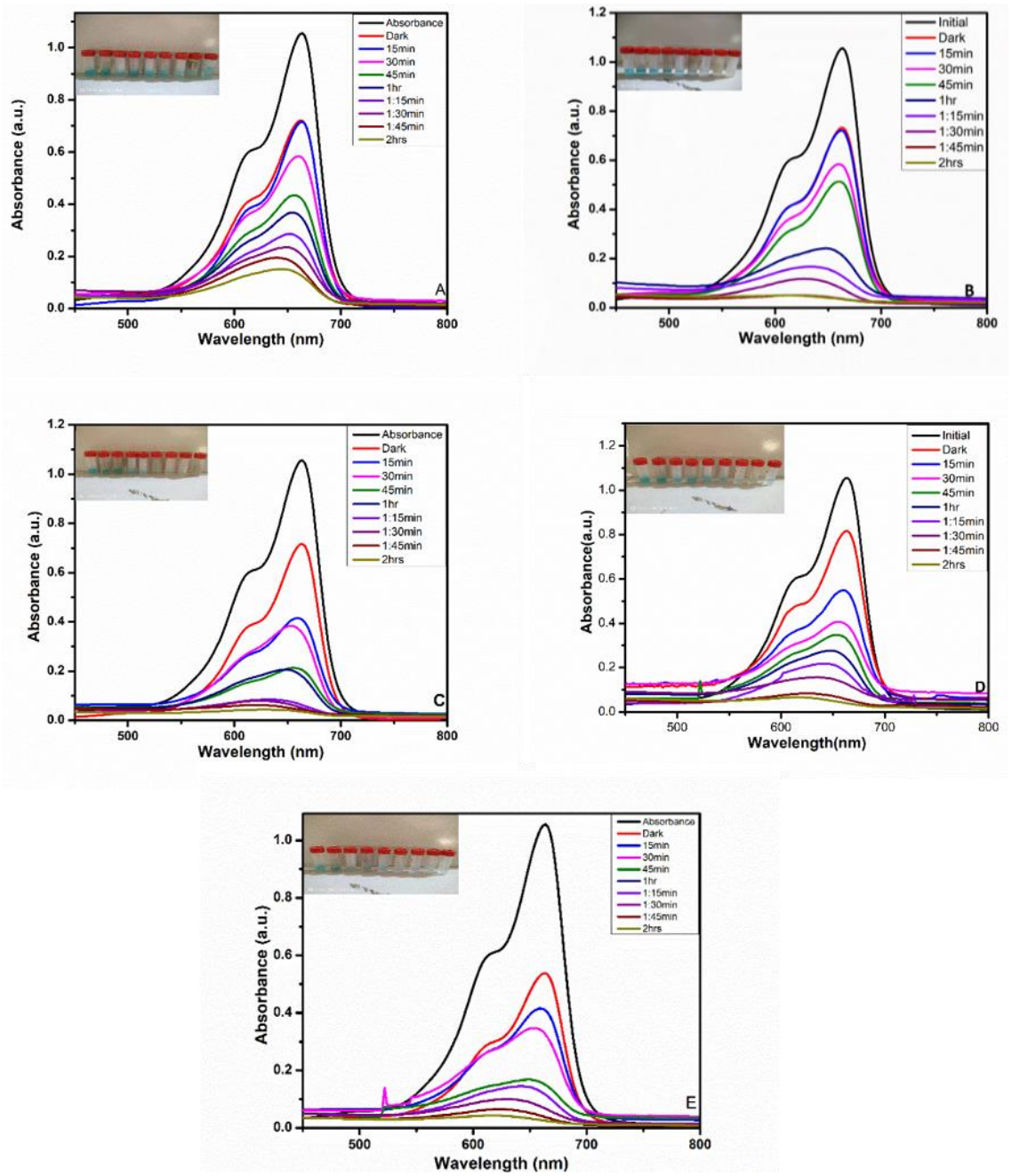


**Figure 8.** Absorbance spectra of MB solution under solar irradiation for (**a**) Pure $SnO_2$, (**b**) 0.25%, (**c**) 0.50%, (**d**) 0.75%, (**e**) 1% Ag/$SnO_2$ nanoparticle.

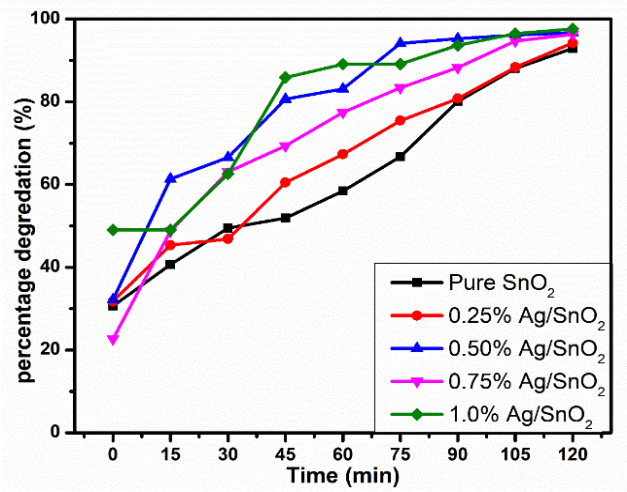


**Figure 9.** Percentage degradation plot of Undoped $SnO_2$, 0.25% Ag/ $SnO_2$, 0.50% Ag/ $SnO_2$, 0.75% Ag/ $SnO_2$, and 1.0% Ag/ $SnO_2$.

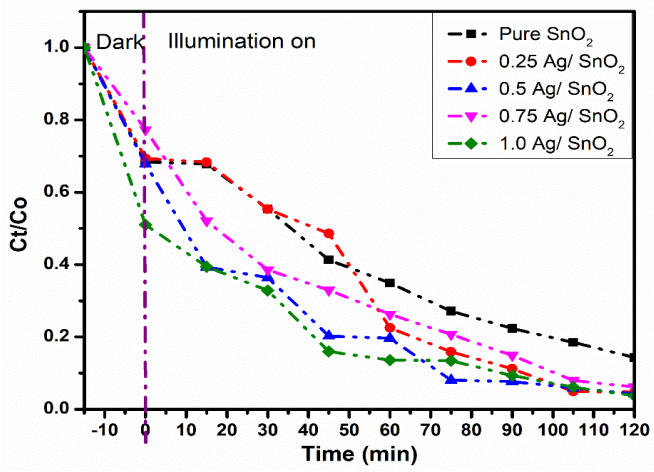


**Figure 10.** Rate of concentration degradation of MB dye against time**.**

*3.7. Mechanism of photocatalysis.*

The mechanism of photocatalysis of undoped $SnO_2$ and Ag-doped $SnO_2$ photocatalyst with MB under solar light is shown in Figure 11. Generally, the production electron and hole (e-/h+) pair are the origin of the photocatalytic degradation method.

During the photocatalytic process, electrons (e-) in the valance band (VB) can be transferred to the conduction band (CB), holes ($h^+$) of the same amount are generated in the VB. These photogenerated ($e^-/h^+$) pairs can aid the chemical reactions with organic pollutants. In the process of chemical reaction, the holes in the VB react with hydroxide ions or $H_2O$ adsorbed at the surface of the photocatalyst to generate hydroxyl radicals (OH). However, electrons in the CB can reduce $O_2$ to make superoxide radicals (*$O_2$-) and subsequently other reactive oxygen species (i.e., $H_2O_2$ and OH-). Consequently, holes and OH as an oxidation agent are immensely reactive toward organic pollutants and positively influence dye degradation [35,46].

$Ag/SnO_2$ showed enhanced photocatalytic performance than undoped $SnO_2$. The enhanced photocatalytic performance was shown by $Ag/SnO_2$ over the undoped $SnO_2$, which can be attributed to the acceptance of impurity by Ag in doping of $SnO_2$, and it acts as an electron trap

that prevents recombination of ($e^-/h^+$), which is a vital influence in determining the photocatalytic performance. Furthermore, the synergy interaction of enhanced visible light absorption, the presence of electron traps in Ag/ $SnO_2$, and visible light-assisted plasmon resonance play a helpful role in enhancing photocatalytic activity [31]. Moreover, Ag/$SnO_2$ has a higher electron reaction with adsorbed O2 than undoped $SnO_2$. Also, the narrow bandgap is another important factor to enhance the photocatalytic activity of $SnO_2$. These results show an efficient photocatalytic activity of the Ag/$SnO_2$.

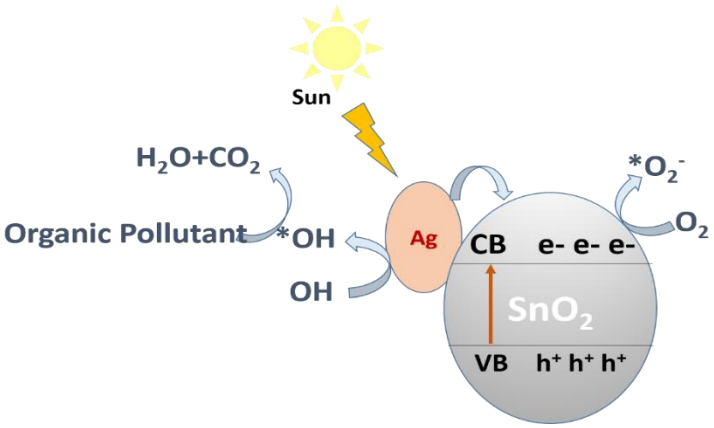


**Figure 11.** Mechanism of photocatalysis of Ag/$SnO_2$ nanoparticles.

## 4. Conclusions

In summary, the coprecipitation method has successfully prepared undoped and Ag/SnO2 NPs at a lower doping concentration of silver below 1%. The incorporation of Ag into $SnO_2$ has been successfully revealed in the XRD pattern. Also, the optical properties showed the effect of Ag doping into $SnO_2$, thereby narrowing the bandgap of $SnO_2$. The Raman spectroscopy also showed the successful incorporation of Ag into the $SnO_2$ lattice. A notable photocatalytic performance towards MB dye solutions were recorded to be 86.89, 94.21, 96.68, 96.30 and 97.63 for undoped, 0.25, 0.5, 0.75 and 1% Ag/$SnO_2$ NPs respectively. It was revealed in the photocatalytic results that a lower doping concentration of Ag into $SnO_2$ has an enhanced photocatalytic performance when compared with existing literature. The improved photocatalytic performance could be attributed to the narrower bandgap of Ag/$SnO_2$. Therefore, a lower doping concentration of Ag has proved effective in the degradation of MB dye under solar light irradiation.

## Funding

This research received no external funding.

## Acknowledgment

OA gratefully acknowledges the Department of Science & Technology (Govt. of India) for the award of the 2019/2020 Research Training Fellowship for Developing Countries Scientist (RTF-DCS). The authors acknowledge with gratefulness the Centre for High-Pressure Research, Bharathidasan University, India, for samples characterizations.

## Conflicts of Interest

The authors declared no conflict of interest.

## References


1. Zhang, J.; Huang, Z.-H.; xu, Y.; Kang, F. Hydrothermal Synthesis of Iodine-Doped Bi 2 WO 6 Nanoplates with Enhanced Visible and Ultraviolet-Induced Photocatalytic Activities. *International Journal of Photoenergy* **2012**, *2012*, https://doi.org/10.1155/2012/915386.
2. Chakhtouna, H.; Benzeid, H.; Zari, N.; Qaiss, A.E.K.; Bouhfid, R. Recent progress on Ag/TiO(2) photocatalysts: photocatalytic and bactericidal behaviors. *Environmental science and pollution research international* **2021**, *28*, 44638-44666, https://doi.org/10.1007/s11356-021-14996-y.
3. Al-Enazi, N.M.; Ameen, F.; Alsamhary, K.; Dawoud, T.; Al-Khattaf, F.; AlNadhari, S. Tin oxide nanoparticles (SnO2-NPs) synthesis using Galaxaura elongata and its anti-microbial and cytotoxicity study: a greenery approach. *Appl. Nanosci.* **2021**, https://doi.org/10.1007/s13204-021-01828-1.
4. Perumal, V.; Inmozhi, C.; Uthrakumar, R.; Robert, R.; Chandrasekar, M.; Mohamed, S.B.; Honey, S.; Raja, A.; Al-mekhlafi, F.A.; Kaviyarasu, K. Enhancing the photocatalytic performance of surface - Treated $SnO_2$ hierarchical nanorods against methylene blue dye under solar irradiation and biological degradation. *Environ. Res.* **2022**, *209*, 112821, https://doi.org/10.1016/j.envres.2022.112821.
5. Wang, Z.; Huang, B.; Dai, Y.; Qin, X.; Zhang, X.; Wang, P.; Liu, H.; Yu, J. Highly photocatalytic $ZnO/In_2O_3$ heteronanostructures synthesized by a coprecipitation method. *J. Phys. Chem. C* **2009**, *113*, 4612–4617, https://doi.org/10.1021/jp8107683.
6. Sujatmiko, F.; Sahroni, I.; Fadillah, G.; Fatimah, I. Visible light-responsive photocatalyst of $SnO_2$/rGO prepared using Pometia pinnata leaf extract. *Open Chem.* **2021**, *19*, 174–183, https://doi.org/10.1515/chem-2020-0117.
7. Sun, L.; Wu, W.; Yang, S.; Zhou, J.; Hong, M.; Xiao, X.; Ren, F.; Jiang, C. Template and silica interlayer tailorable synthesis of spindle-like multilayer $\alpha$-$Fe_2O_3$/Ag/$SnO_2$ ternary hybrid architectures and their enhanced photocatalytic activity. *ACS Appl. Mater. Interfaces* **2014**, *6*, 1113–1124, https://doi.org/10.1021/am404700h.
8. Ahmed, M.K.; Shalan, A.E.; Afifi, M.; El-Desoky, M.M.; Lanceros-Méndez, S. Silver-Doped Cadmium Selenide/Graphene Oxide-Filled Cellulose Acetate Nanocomposites for Photocatalytic Degradation of Malachite Green toward Wastewater Treatment. *ACS Omega* **2021**, *6*, 23129–23138, https://doi.org/10.1021/acsomega.1c02667.
9. Zhang, Z.; Shao, C.; Li, X.; Zhang, L.; Xue, H.; Wang, C. Electrospun Nanofibers of ZnO - $SnO_2$ Heterojunction with High Photocatalytic Activity. *J. Phys. Chem. C* **2010**, 7920–7925, https://doi.org/10.1021/jp100262q.
10. Qin, Q.; Wang, J.; Xia, Y.; Yang, D.; Zhou, Q.; Zhu, X.; Feng, W. Synthesis and Characterization of Sn/Ni Single Doped and Co–Doped Anatase/Rutile Mixed–Crystal Nanomaterials and Their Photocatalytic Performance under UV–Visible Light. *Catalysts* **2021**, *11*, 1341, https://doi.org/10.3390/catal11111341.
11. Stasinakis, A. Use of Selected Advanced Oxidation Processes (AOPs) for Wastewater Treatment – a Mini Review. *Global NEST Journal Copyright©* **2008**, *10*, 376-385.
12. Zhu, S.; Wang, D. Photocatalysis: Basic principles, diverse forms of implementations and emerging scientific opportunities. *Adv. Energy Mater.* **2017**, *7*, 1–24, https://doi.org/10.1002/aenm.201700841.
13. Ansari, S.A.; Khan, M.M.; Ansari, M.O.; Lee, J.; Cho, M.H. Visible light-driven photocatalytic and photoelectrochemical studies of Ag-$SnO_2$ nanocomposites synthesized using an electrochemically active biofilm. *RSC Adv.* **2014**, *4*, 26013–26021, https://doi.org/10.1039/c4ra03448a.
14. Bessegato, G.G.; Guaraldo, T.T.; Zanoni, M.V.B. Enhancement of Photoelectrocatalysis Efficiency by Using Nanostructured Electrodes. *Mod. Electrochem. Methods Nano, Surf. Corros. Sci*. **2014**, https://doi.org/10.5772/58333.
15. Chan, S.H.S.; Wu, T.Y.; Juan, J.C.; Teh, C.Y. Recent developments of metal oxide semiconductors as photocatalysts in advanced oxidation processes (AOPs) for treatment of dye wastewater. *J. Chem. Technol. Biotechnol.* **2011**, *86*, 1130–1158, https://doi.org/10.1002/jctb.2636.

16. Nadumane, A.; Shetty, K.; Anantharaju, K.S.; Nagaswarupa, H.P.; Rangappa, D.; Vidya, Y.S.; Nagabhushana, H.; Prashantha, S.C. Sunlight photocatalytic performance of Mg-doped nickel ferrite synthesized by a green sol-gel route. *J. Sci. Adv. Mater. Devices* **2019**, *4*, 89–100, https://doi.org/10.1016/j.jsamd.2018.12.002.
17. Vignesh, K.; Hariharan, R.; Rajarajan, M.; Suganthi, A. Photocatalytic performance of Ag doped $SnO_2$ nanoparticles modified with curcumin. *Solid State Sci.* **2013**, *21*, 91–99, https://doi.org/10.1016/j.solidstatesciences.2013.04.017.
18. Joshi, N.C.; Gururani, P.; Gairola, S.P. Metal oxide nanoparticles and their nanocomposite-based materials as photocatalysts in the degradation of dyes. *Biointerface Res. Appl. Chem*. **2022**, *12*, 6557–6579, https://doi.org/10.33263/BRIAC125.65576579.
19. Gebreslassie, Y.T.; Gebretnsae, H.G. Green and Cost-Effective Synthesis of Tin Oxide Nanoparticles: A Review on the Synthesis Methodologies, Mechanism of Formation, and Their Potential Applications. *Nanoscale Res. Lett.* **2021**, *16*, 1–16, https://doi.org/10.1186/s11671-021-03555-6.
20. Teoh, W.Y.; Scott, J.A.; Amal, R. Progress in heterogeneous photocatalysis: From classical radical chemistry to engineering nanomaterials and solar reactors. *J. Phys. Chem. Lett*. **2012**, *3*, 629–639, https://doi.org/10.1021/jz3000646.
21. Yin, K.; Shao, M.; Zhang, Z.; Lin, Z. A single-source precursor route to Ag/$SnO_2$ heterogeneous nanomaterials and its photocatalysis in degradation of Conco Red. *Mater. Res. Bull*. **2012**, *47*, 3704–3708, https://doi.org/10.1016/j.materresbull.2012.06.037.
22. Liu, H.; Dong, X.; Duan, C.; Su, X.; Zhu, Z. Silver-modified $TiO_2$ nanorods with enhanced photocatalytic activity in visible light region. *Ceram. Int.* **2013**, *39*, 8789–8795, https://doi.org/10.1016/j.ceramint.2013.04.066.
23. Awoke, N.; Pandey, D.; Habtemariam, A.B. Synthesis of Tin(IV) Oxide Nanoparticles Using Plant Leaf Extracts of Vernonia amygdalina and Mentha spicata. *Regen. Eng. Transl. Med.* **2021**, https://doi.org/10.1007/s40883-021-00218-x.
24. Wang, H. Photochemical Preparation of Ag/$SnO_2$ Composites and their Photocatalytic Properties. **2015**, 326–329.
25. Li, G.-S.; Zhang, D.; Yu, J. A New Visible-Light Photocatalyst: CdS Quantum Dots Embedded Mesoporous TiO2. *Environmental science & technology* **2009**, *43*, 7079-7085, https://doi.org/10.1021/es9011993.
26. Sun, S.; Meng, G.; Zhang, G.; Zhang, L. Controlled Growth and Optical Properties of One-Dimensional ZnO Nanostructure on $SnO_2$ Nanobelts *Cryst. Growth Des.* **2007**, *7*, 1988-1991, https://doi.org/10.1021/cg0701776
27. Wen, Z.; Wang, G.; Lu, W.; Wang, Q.; Zhang, Q.; Li, J. Enhanced photocatalytic properties of mesoporous $SnO_2$ induced by low concentration ZnO doping. *Cryst. Growth Des.* **2007**, *7*, 1722–1725, https://doi.org/10.1021/cg060801z.
28. Wu, W.; Liao, L.; Zhang, S.; Zhou, J.; Xiao, X.; Ren, F.; Sun, L.; Dai, Z.; Jiang, C. Non-centrosymmetric Au-SnO2 hybrid nanostrutures with strong localization of plasmonic for enhanced photocatalysis application. *Nanoscale* **2013**, *5*, https://doi.org/10.1039/c3nr00985h.
29. Elizabeth Sunny, N.; Kumar Shanmugam, V. Anti- blight effect of green synthesized pure and Ag-doped tin oxide nanoparticles from Averrhoa bilimbi fruit extract towards Xanthomonas oryzae-the leaf blight pathogen of rice. *Inorg. Chem. Commun*. **2021**, *133*, 108866, https://doi.org/10.1016/j.inoche.2021.108866.
30. Xu, S.; Li, D.; Guo, J.; Hu, Y.; Yang, P. Aluminum and silver doped effects on the electrical structure and optical properties of $SnO_2$. *J. Phys. Chem. Solids* **2021**, *148*, 109763, https://doi.org/10.1016/j.jpcs.2020.109763.
31. Parthibavarman, M. Microwave Assisted Synthesis of Pure and Ag Doped $SnO_2$ Quantum Dots as Novel Platform for High Photocatalytic Activity Performance. *J. Clust. Sci.* **2019**, *5*, https://doi.org/10.1007/s10876-018-01493-5.
32. Yadav, S.; Mittal, A.; Sharma, S.; Sharma, A.; Kumari, K.; Kumar, N. Ag sensitized ZnO/$SnO_2$ heterostructures for photocatalytic decontamination of water. *Appl. Nanosci.* **2021**, *11*, 2537–2547, https://doi.org/10.1007/s13204-021-02102-0.
33. Kareem, M.A.; Bello, I.T.; Shittu, H.A.; Sivaprakash, P.; Adedokun, O.; Arumugam, S. Synthesis, characterization, and photocatalytic application of silver doped zinc oxide nanoparticles. *Clean. Mater*. **2022**, *3*, 100041, https://doi.org/10.1016/j.clema.2022.100041.

34. Bui, D.P.; Nguyen, M.T.; Tran, H.H.; You, S.; Wang, Y.; Viet, P. Van Green synthesis of Ag@$SnO_2$ nanocomposites for enhancing photocatalysis of nitrogen monoxide removal under solar light irradiation. *Catal. Commun.* **2019**, 105902, https://doi.org/10.1016/j.catcom.2019.105902.
35. Sinha, T.; Adhikari, P.P.; Bora, R. Green and Environmentally Sustainable Fabrication of Ag-$SnO_2$ Nanocomposite and Its Multifunctional Efficacy As Photocatalyst and Antibacterial and Antioxidant Agent. *ACS Sustain. Chem. Eng.* **2017**, https://doi.org/10.1021/acssuschemeng.6b03114.
36. Ma, Y.; Tao, L.; Bai, S.; Hu, A. Green Synthesis of Ag Nanoparticles for Plasmon-Assisted Photocatalytic Degradation of Methylene Blue. *Catalysts* **2021**, *111*, 1–14, https://doi.org/10.3390/catal11121499.
37. Fatimah, I.; Purwiandono, G.; Hidayat, H.; Sagadevan, S.; Ghazali, S.A.I.S.M.; Oh, W.C.; Doong, R.A. Flower-like $SnO_2$ nanoparticle biofabrication using pometia pinnata leaf extract and study on its photocatalytic and antibacterial activities. *Nanomaterials* **2021**, *11*, 1–17, https://doi.org/10.3390/nano11113012.
38. Rekha, K.; Nirmala, M.; Nair, M.G.; Anukaliani, A. Structural, optical, photocatalytic and antibacterial activity of zinc oxide and manganese doped zinc oxide nanoparticles. *Physica B: Condensed Matter* **2010**, *405*, 3180-3185, https://doi.org/10.1016/j.physb.2010.04.042.
39. Obeızı, Z.; Benbouzid, H.; Bouarroudj, T.; Chahrazed, B.; Abdelghani, D. Synthesis, characterization of (Ag-SnO2) Nanoparticles and Investigation of Its Antibacterial and Anti-Biofilm Activities. *Journal of New Technology and Materials* **2021**, *10*, https://doi.org/10.12816/0058531.
40. Nasir, Z.; Shakir, M.; Wahab, R.; Shoeb, M.; Alam, P. Coprecipitation synthesis and characterization of Co doped $SnO_2$ NPs , HSA interaction via various spectroscopic techniques and their antimicrobial and photocatalytic activities International Journal of Biological Macromolecules Coprecipitation synthesis. *Int. J. Biol. Macromol.* **2018**, *94*, 554–565, https://doi.org/10.1016/j.ijbiomac.2016.10.057.
41. Yakout, S.M. Inclusion of cobalt reinforced Ag doped $SnO_2$ properties: electrical, dielectric constant, magnetic and photocatalytic insights. *J. Mater. Sci. Mater. Electron*. **2019**, *30*, 17053–17065, https://doi.org/10.1007/s10854-019-02052-y.
42. Senthil Kumar, P.; Selvakumar, M.; Babu, S.G.; Jaganathan, S.K.; Karuthapandian, S.; Chattopadhyay, S. Novel CuO/chitosan nanocomposite thin film: facile hand-picking recoverable, efficient and reusable heterogeneous photocatalyst. *RSC Advances* **2015**, *5*, 57493-57501, https://doi.org/10.1039/C5RA08783J.
43. Rattan, S.; Suresh, K.; Mamta, S.; Tripathi, S.K.; Goswamy, J. Synthesis and characterization of Ag Metal doped $SnO_2$, $WO_3$ and $WO_3$-$SnO_2$ for Propan-2-ol sensing. *Results Mater.* **2020**, 100127, https://doi.org/10.1016/j.rinma.2020.100127.
44. Liu, H.; Hu, Y.; Zhang, Z.; Liu, X.; Jia, H.; Xu, B. Synthesis of spherical Ag/ZnO heterostructural composites with excellent photocatalytic activity under visible light and UV irradiation. *Appl. Surf. Sci.* **2015**, *355*, 644–652, https://doi.org/10.1016/j.apsusc.2015.07.012.
45. Islam, M.R.; Rahman, M.; Farhad, S.F.U.; Podder, J. Structural , optical and photocatalysis properties of sol – gel deposited Al- doped ZnO thin films. *Surfaces and Interfaces* **2019**, *16*, 120–126, https://doi.org/10.1016/j.surfin.2019.05.007.
46. Manjula, N.; Selvan, G.; Balu, A.R. Improved photodegradation activity of $SnO_2$ nanopowder against methyl orange dye through Ag doping. *J. Mater. Sci. Mater. Electron.* **2018**, *29*, 3657–3664, https://doi.org/10.1007/s10854-017-8296-1.
47. Wang, X.; Fan, H.; Ren, P. Colloids and Surfaces A: Physicochemical and Engineering Aspects Self-assemble flower-like $SnO_2$/Ag heterostructures : Correlation among composition , structure and photocatalytic activity highlights. *Colloids Surfaces A Physicochem. Eng. Asp.* **2013**, *419*, 140–146, https://doi.org/10.1016/j.colsurfa.2012.11.050.
48. Liu, H.; Liu, T.; Dong, X.; Hua, R.; Zhu, Z. Preparation and enhanced photocatalytic activity of Ag-nanowires @ $SnO_2$ core – shell heterogeneous structures. *Ceram. Int.* **2014**, *40*, 16671–16675, https://doi.org/10.1016/j.ceramint.2014.08.029.